PERFORMANCE BOUNDS FOR DISPLACED SENSOR AUTOMOTIVE RADAR IMAGING

Guohua Wang[1] *and Kumar Vijay Mishra*[1,2]

[1]Hertzwell Pte Ltd, Singapore 138565
[2]The University of Iowa, Iowa City, IA 52242 USA

ABSTRACT

In automotive radar imaging, displaced sensors offer improvement in localization accuracy by jointly processing the data acquired from multiple radar units, each of which may have limited individual resources. In this paper, we derive performance bounds on the estimation error of target parameters processed by displaced sensors that correspond to several independent radars mounted at different locations on the same vehicle. Unlike previous studies, we do not assume a very accurate time synchronization among the sensors. Instead, we consider only frame-level time alignment which is more common and practical in modern automotive sensor networks. We first develop a displaced multiple-input multiple-output (MIMO) frequency-modulated continuous-wave (FMCW) radar signal model under coarse synchronization and then propose processing models relevant to modern automotive radars such as point-cloud-based fusion and raw signal imaging. Contrary to earlier works based on deterministic Cramér-Rao lower bound, our displaced sensors framework is Bayesian. Numerical experiments with our proposed non-coherent processing of displaced MIMO FMCW radars show an order of performance improvement in position estimation over the conventional point-cloud fusion.

Index Terms— Automotive radar, Bayesian Cramér-Rao lower bound, displaced sensors, high-resolution, synchronization.

1. INTRODUCTION

High-resolution sensing is a critical enabling technology for enhancing the safety of autonomous vehicles [1]. To this end, self-driving cars employ a number of sensors such as camera, radar, lidar and ultrasonics to provide either individual or joint information from the surroundings [2]. Although camera is favorable for object detection and lidar provides high range resolution, only radar performs well in unfavorable conditions such as inclement weather and low visibility [3]. It is possible to offset the comparatively low spatial resolution offered by the radar by increasing its transmit signal bandwidth, coherent processing interval (CPI) or frame time [4], and antenna aperture size [5]; however, limited frequency spectrum at millimeter-wave (mm-Wave) [5, 6], lower frame rate from increased frame times [1], and requirement of small form factor restrict adoption of each of these measures [7–9], respectively. In this context, the idea of deploying multiple radars on the same vehicle and then jointly processing their data to achieve high-resolution has attracted significant attention lately within the automotive radar community [10, 11].

There is a large body of literature on distributed sensors for communications [12–14] and radars [15, 16]. These approaches for joint processing broadly follow two techniques. In *geolocation database* method, cross-correlation of measurements of parameters such as directions-of-arrival (DOAs), time-differences-of-arrival (TDOAs), times-of-arrival (TOAs), and frequency-differences-of-arrival (FDOAs) of a radio-frequency (RF) signal received by multiple distributed sensors is used to retrieve the position of a target [17–19]. The geolocation approach does not require complex hardware and is easier to implement. But it is inherently a two-step processing - a measurement step followed by position acquisition. Thus, the errors in each step propagate, thereby limiting the accuracy. This shortcoming is eliminated by employing direct position determination (DPD) [15, 20] which infers geolocation directly from raw data. Nearly all of these methods assume that the distributed sensors are perfectly synchronized or their receiver clock offsets are known, which is not feasible in [21]. To alleviate this problem, some recent studies [22, 23] developed procedures for source localization in communications by performing DOA estimation and DPD of multiple stationary RF transmitters without time synchronization. In the context of radar, [24] suggested non-coherent processing using compressed sensing (CS) [25] to estimate target positions for widely distributed radars without synchronization. However, it exploits only range information and is inferior compared to techniques which additionally blend other parameters such as DOA.

Further, geolocation approaches do not yield accurate estimates of target reflectivity. This has led to the development of *distributed imaging* algorithms which yield both target position and reflectivity. Recently, [26] proposed a CS-based high-resolution multi-static radar imaging using raw data in spectral domain; perfect synchronization and perfect knowledge of sensor geometry was assumed. More recently, an interesting study [27] on coherent radar imaging using unsynchronized distributed antennas modeled errors in time synchronization and antenna positions to accurately estimate target reflectivity and position. However, this work did not provide any theoretical guarantees. Further, for automotive radars, the assumption on bounded time synchronization errors is impractical [21]. In this paper, contrary to prior works, we derive theoretical performance limits of displaced radar imaging, assume imperfect synchronization, and apply automotive-specific system details.

In our model, different from a conventional distributed multiple-input multiple-output (MIMO) radar [28], the automotive displaced sensors operate independently and are only *coarsely* time-synchronized through use of standards such as IEEE 1588 generic precision time protocol (gPTP) [29]. These protocols provide synchronization accuracy of microseconds, which is quite coarse compared to the conventional TDOA-based localization and positioning. Each radar being independent, our received signal depends only on the local timing of each sensor thereby circumventing the need of fine inter-sensor time-synchronization. In this case, the imaging algorithms still provide an improved performance by combining data from individual radar sensors. To this end, we assume that prior information from high-definition maps or previous imaging output of each radar is also available so as to enable analysis of our displaced radar system in a Bayesian framework.

The rest of the paper is organized as follows. In the next section, we describe the coarse synchronization signal model for the con-

This work was funded by Hertzwell Pte Ltd.

ventional frequency-modulated continuous-wave (FMCW) MIMO radar operating in time-division multiplexing (TDM) mode. For this system, we introduce three processing modes relevant to the automotive radar imaging: point-cloud fusion, coherent and non-coherent processing. We then derive the Bayesian Cramér-Rao lower bound (BCRLB)[1] [32, 33] for estimating the position in these modes in Section 3 and compare them through numerical experiments in Section 4. We conclude in Section 5.

Throughout this paper, we denote boldface lowercase, boldface uppercase and calligraphic letters for vectors, matrices and index sets, respectively. The notation $(\cdot)^H$ stands for conjugate transpose and transpose for complex and real quantities, respectively. The Kronecker and Hadamard products are written as $\otimes$ and $\circ$, respectively. We use $\mathbf{1}_N$ for the vector of size $N \times 1$. The functions $\Re(\cdot)$ and $\Im(\cdot)$ yield the real and imaginary parts of their arguments; *diag*$\{\mathbf{a}\}$ is a diagonal matrix formed from the elements of vector $\mathbf{a}$; and $\mathbb{E}\{\cdot\}$ is the statistical expectation.

2. SYSTEM MODEL

Consider a displaced automotive radar system (Fig. 1) with Q sensors mounted on different locations of a single vehicle. Without loss of generality, each radar is a MIMO array with N transmit and M receive antennas. The center-of-mass of the vehicle is the global reference position (or origin) across this system. In this two-dimensional (2-D) coordinate system, the positions of transmit and receive antennas of the q-th radar are $\mathbf{p}^q_{T,n} = [x_{q,n}; y_{q,n}] \in \mathbb{R}^{2\times 1}, n = 1, \cdots, N$ and $\mathbf{p}^q_{R,m} = [x_{q,m}; y_{q,m}] \in \mathbb{R}^{2\times 1}, m = 1, \cdots, M$, respectively. The radars employ TDM transmission among different transmit antennas. This is a widely adopted waveform orthogonality in automotive MIMO radars [2]. The cross-interference between individual radar sensors is avoided by separating the transmit spectrum of each radar through frequency diversity [4].

Each q-th radar transmitter emits K FMCW chirps, each of duration T_p, at a pulse repetition interval T_r and carrier frequency f^q_c and modulation rate B_r. The frame time (or CPI) comprises NK sweeps from all transmitters. The proposed system here does not require high-precision synchronization and it is achieved only coarsely through use of gPTP. The coarse clock implies that for a global time reference t, the time offset with the local time t_q of q-th radar is σ_q so that $t_q = t - \sigma_q$. The σ_q is very small, usually of the order of milliseconds. As a consequence, the radar and target positions are assumed to be constant across all different radar sensors during a CPI [34]. The transmit waveform at k-th pulse and n-th transmit antenna of the q-th radar sensor is

$$s_{q,n}(t,k) = \text{rect}\left(\frac{t-\sigma_q}{T_p}\right) e^{j2\pi f^q_c (t-\sigma_q+(n-1+(k-1)N)T_r)} e^{j\pi B_r (t-\sigma_q)^2}, \quad k = 0, \cdots, K \tag{1}$$

where $\text{rect}(t)$ is the rectangular pulse function

$$\text{rect}(t) = \begin{cases} 1, & t \in [0,1] \\ 0, & \text{otherwise.} \end{cases} \tag{2}$$

The transmit chirps impinge a target at position $\mathbf{p}_t = [x; y] \in \mathbb{R}^{2\times 1}$ moving at a velocity $\mathbf{v}_t \in \mathbb{R}^{2\times 1}$ relative to the vehicle. Then, the target Doppler velocity is $v_q = \mathbf{v}^H_t \mathbf{p}_{t,q}$, where $\mathbf{p}_{t,q}$ denotes the direction vector between the q-th radar and target. Denoting the speed

[1]Note that BCRLB is different from the *hybrid* CRLB (HCRLB) [30, 31] where parameter vector has both random and deterministic variables.

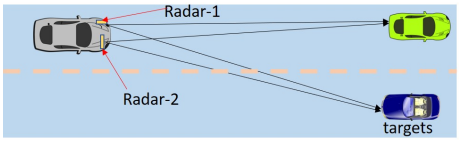

Fig. 1. An automotive displaced sensor system employs multiple radars ('Radar-1' and 'Radar-2') that are mounted on different locations of the same vehicle (grey) and jointly observe common targets (red and green vehicles).

of light as c, the bistatic time delay from the n-th transmitter to target and back to the m-th receiver of the q-th radar sensor is

$$\tau_{q,m,n}(t,k) = \frac{g_{q,m,n}}{c} + 2v_q(t + (n-1+(k-1)N)T_r)/c, \tag{3}$$

where the bistatic range $g_{q,m,n} = g^q_{T,n} + g^q_{R,m}$ with

$$g^q_{T,n} = ||\mathbf{p}_t - \mathbf{p}^q_{T,n}|| = ((x_{q,n}-x)^2 + (y_{q,n}-y)^2)^{1/2}, \tag{4}$$

$$g^q_{R,m} = ||\mathbf{p}_t - \mathbf{p}^q_{R,m}|| = ((x_{q,m}-x)^2 + (y_{q,m}-y)^2)^{1/2}. \tag{5}$$

The target follows the Swerling-1 model [35] so that its unknown reflection coefficient $\tilde{\alpha}_q$ remains constant across one CPI.

The signal reflected off the target and received at m-th antenna is

$$s_{q,m,n}(t,k) = \tilde{\alpha}_q \text{rect}\left(\frac{t-\sigma_q-\tau_{q,m,n}(t,k)}{T_p}\right) e^{j2\pi f^q_c (t-\sigma_q-\tau_{q,m,n}(t,k)+(n-1+(k-1)N)T_r)} e^{j\pi B_r (t-\sigma_q-\tau_{q,m,n}(t,k))^2}. \tag{6}$$

The FMCW receiver mixes this signal with the transmit waveform of the same radar transmitter to produce the baseband signal

$$\tilde{y}_{q,m,n}(t,k) = \tilde{\alpha}_q \text{rect}\left(\frac{t-\sigma_q-\tau_{q,m,n}(t,k)}{T_p}\right) e^{-j2\pi f^q_c \tau_{q,m,n}(t,k)} e^{j\pi B_r(-2(t-\sigma_q)\tau_{q,m,n}(t,k)+\tau^2_{q,m,n}(t,k))}. \tag{7}$$

Changing the variables $t = t_c + \sigma_q$ with $t_c = t_q$ yields

$$\tilde{y}_{q,m,n}(t_c,k) = \tilde{\alpha}_q \text{rect}\left(\frac{t_c-\tau_{q,m,n}(t_c+\sigma_q,k)}{T_p}\right) e^{-j2\pi f^q_c \tau_{q,m,n}(t_c+\sigma_q,k)} e^{j\pi B_r(-2(t_c)\tau_{q,m,n}(t_c+\sigma_q,k)+\tau^2_{q,m,n}(t_c+\sigma_q,k))}. \tag{8}$$

Substituting delay expression and omitting higher order phases gives

$$y_{q,m,n}(t_c,k) = \tilde{\alpha}_q c_q e^{-j2\pi f^q_c g_{q,m,n}/c} e^{-j2\pi\left(\frac{2f^q_c v_q}{c} + \frac{B_r g_{q,m,n}}{c}\right)t_c} e^{-j2\pi \frac{2f^q_c v_q T_r}{c}(n-1+(k-1)N))}, \tag{9}$$

where $c_q = e^{-j2\pi f^q_c \frac{2v_q}{c}\sigma_q}$ is the complex phase term due to σ_q.

In (9), we used t_c to replace t_q because the relative local timing at different sensors is same. This implies that when each radar sensor is synchronized within itself, the received signal model - except for a complex phase term - depends on only local time which is same for all radars. This holds as long as the frame time of different radars are coarsely synchronized. In addition, the above calculations reveal that the time synchronization primarily affects the Doppler frequency and DOA estimates when performing coherent estimate across multiple

sensors. For static target and radar, the model is identical for both synchronous and asynchronous operations. Thus, incorporating the time synchronization induced phase term c_q into the signal amplitude, i.e., $\alpha_q = \tilde{\alpha}_q c_q$ simplifies the static scenario model as

$$s_{q,m,n}(t_c) = \alpha_q K e^{-j2\pi(f_c^q + \frac{B_r}{c} t_c) g_{q,m,n}/c} \triangleq \alpha_q h_{q,m,n}(t_c). \tag{10}$$

We now consider three different automotive radar techniques to jointly process the received signal. Later, we evaluate the statistical bounds for each of these three methods.

Point-cloud fusion: A point-cloud generated at each q-th radar sensor provides estimates of target's range, DOA, Doppler, and amplitude as $\{\hat{r}_q, \hat{\theta}_q, \hat{v}_q, \hat{\alpha}_q\}$. The estimation accuracy of these parameters is improved by fusing the point-clouds of each sensor. The displaced sensor imaging refines the target estimation based on the set of measurements from all sensors. For example, consider the estimation of target position. Then, the point-cloud fusion exploits both $\hat{r}_q$ and $\hat{\theta}_q$ as follows. Define $\mathbf{\Phi} = [x, y]^T$ as the unknown parameter vector of target position. The estimates of range and DOA are modeled as

$$\hat{r}_q = r_q(\mathbf{\Phi}) + n_{r,q},\ \hat{\theta}_q = \theta_q(\mathbf{\Phi}) + n_{\theta,q}, \tag{11}$$

where $n_{r,q}$ and $n_{\theta,q}$ are the measurement noises. The range and DOA measurements at the q-th radar are, respectively,

$$r_q(\mathbf{\Phi}) = ((x - x_{q,1})^2 + (y - y_{q,1})^2)^{1/2}, \tag{12}$$

$$\theta_q(\mathbf{\Phi}) = tan^{-1}\left(\frac{y - y_{q,1}}{x - x_{q,1}}\right). \tag{13}$$

Stacking measurements from all Q radars, we get

$$\mathbf{z} = \mathbf{f}(\mathbf{\Phi}) + \mathbf{n}, \tag{14}$$

where $\mathbf{z} = [\hat{r}_1, \cdots, \hat{r}_Q, \hat{\theta}_1, \cdots, \hat{\theta}_Q]^T$, $\mathbf{f}(\mathbf{\Phi}) = [r_1(\mathbf{\Phi}), \cdots, r_Q(\mathbf{\Phi}), \theta_1(\mathbf{\Phi}), \cdots, \theta_Q(\mathbf{\Phi})]^T$, and $\mathbf{n} \sim N(\mathbf{0}, \mathbf{R}_n)$ is Gaussian noise. The probability density function of the measurements $\mathbf{z}$ is $p(\mathbf{z}, \mathbf{\Phi}) = p(\mathbf{z}|\mathbf{\Phi})p_o(\mathbf{\Phi})$. The point-cloud fusion aims at improving the accuracy of the estimation of $\mathbf{\Phi}$ by maximizing the posterior distribution.

Non-coherent processing: Here, each radar sensor is so widely distributed than the other sensors that it observes a different amplitude and phase of target reflectivity. In the presence of noise, these non-coherent measurements at time instant $t \in \{t_1, \cdots, t_{N_s}\}$

$$z_{q,m,n}(t) = \alpha_q h_{q,m,n}(t) + n_{q,m,n}(t), \tag{15}$$

stacked in a single vector are $\mathbf{z}_{nc} = [z_{1,1,1}(t_1), \cdots, z_{Q,M,N}(t_{N_s})]^T$. This received signal vector is expanded as

$$\mathbf{z}_{nc} = (\boldsymbol{\alpha} \otimes \mathbf{1}_{MNN_s}) \circ \mathbf{h}(\mathbf{\Phi}) + \mathbf{n}_{nc}, \tag{16}$$

where $\boldsymbol{\alpha} = [\alpha_1, \cdots, \alpha_Q]^T$ and $\mathbf{h}(\mathbf{\Phi}) = [h_{1,1,1}(t_1), \cdots, h_{Q,M,N}(t_{ns})]$. We further define $\mathbf{\Phi}_1 = [\mathbf{\Phi}^T, \boldsymbol{\alpha}]^T$. The noise follows circular symmetric Gaussian distribution, i.e., $\mathbf{n}_{nc} \sim \mathcal{CN}(\mathbf{0}, \mathbf{R}_{nc})$ and α_q are i.i.d Gaussian random variables following $\alpha_q \sim \mathcal{CN}(0, \sigma^2)$.The probability density function is conditioned on the amplitude as $p(\mathbf{z}_{nc}, \mathbf{\Phi}|\boldsymbol{\alpha}) = p(\mathbf{z}_{nc}|\mathbf{\Phi}, \boldsymbol{\alpha})p_o(\mathbf{\Phi})$, where $\mathbf{\Phi}$ is independent of $\boldsymbol{\alpha}$, i.e., $p_o(\mathbf{\Phi}) = p_o(\mathbf{\Phi}|\boldsymbol{\alpha})$. The non-coherent processing method estimates the target position based on the posterior probability distribution.

Coherent processing: Here, the antennas are well-calibrated over all radar sensors such that all radars view the target with identical reflectivity. Further, perfect synchronization is assumed so that c_q in (9) is irrelevant here. These assumptions are quite strong for automotive applications but this processing provide best achievable performance bound and serves as a benchmark. The measurements for the coherent processing are

$$\mathbf{x}_c = \alpha \mathbf{h}(\mathbf{\Phi}) + \mathbf{n}_c, \tag{17}$$

where the noise $\mathbf{n}_c \sim \mathcal{CN}(\mathbf{0}, \mathbf{R}_c)$ and $\alpha \sim \mathcal{CN}(0, \sigma^2)$. Assuming the signal parameter α is independent of $\mathbf{\Phi}$, the probability density function is $p(\mathbf{x}_c, \mathbf{\Phi}|\alpha) = p(\mathbf{x}_c|\mathbf{\Phi}, \alpha)p_o(\mathbf{\Phi})$.

3. PERFORMANCE BOUNDS

We now derive BCRLB for each of these three modes based on prior information on $\mathbf{\Phi}$.

Theorem 3.1 (Point-cloud fusion BCRLB)**.** *Given the prior $\mathbf{\Phi} \sim N(\mathbf{\Phi}_o, \mathbf{R_o})$, the BCRLB for point-cloud fusion is the inverse of the Fisher Information Matrix (FIM)*

$$\mathbf{F}_\Phi = \mathbb{E}\{\mathbf{F}_l\} + \mathbf{F}_0, \tag{18}$$

where $\mathbf{F}_l$ and $\mathbf{F}_0$ are determined by deterministic CRLB and prior information, respectively.

Proof: For conventional processing, the deterministic CRLB is based on the likelihood function $p(\mathbf{x}|\mathbf{\Phi})$ as

$$\mathbf{C}_{\hat{\mathbf{\Phi}}} = \mathbb{E}_{\mathbf{x}|\mathbf{\Phi}}\left\{(\mathbf{\Phi} - \hat{\mathbf{\Phi}})(\mathbf{\Phi} - \hat{\mathbf{\Phi}})^T\right\} \succeq \mathbf{F}_l^{-1}, \tag{19}$$

where the FIM $\mathbf{F}_l$ is

$$\mathbf{F}_l = -\mathbb{E}\left\{\frac{\partial^2 \ln p(\mathbf{x}|\mathbf{\Phi})}{\partial \mathbf{\Phi}^2}\right\} = \mathbb{E}\left\{\left(\frac{\partial \ln p(\mathbf{x}|\mathbf{\Phi})}{\partial \mathbf{\Phi}}\right)\left(\frac{\partial \ln p(\mathbf{x}|\mathbf{\Phi})}{\partial \mathbf{\Phi}}\right)^T\right\}. \tag{20}$$

The BCRLB is based on posterior distribution $p(\mathbf{\Phi}|\mathbf{x}) = p(\mathbf{x}|\mathbf{\Phi})p_o(\mathbf{\Phi})$,

$$\mathbf{C}_{\hat{\mathbf{\Phi}}} = \mathbb{E}_{\mathbf{x},\mathbf{\Phi}}\left\{(\mathbf{\Phi} - \hat{\mathbf{\Phi}})(\mathbf{\Phi} - \hat{\mathbf{\Phi}})^T\right\} \succeq \mathbf{F}_\Phi^{-1}, \tag{21}$$

where the Bayesian FIM $\mathbf{F}_\Phi$ for point-cloud fusion processing is [36]

$$\begin{aligned}
\mathbf{F}_\Phi &= -\mathbb{E}_{\mathbf{x},\mathbf{\Phi}}\left\{\frac{\partial^2 \ln p(\mathbf{\Phi}, \mathbf{x})}{\partial \mathbf{\Phi}^2}\right\} \\
&= -\mathbb{E}_{\mathbf{x},\mathbf{\Phi}}\left\{\frac{\partial^2 \ln p(\mathbf{x}|\mathbf{\Phi})}{\partial \mathbf{\Phi}^2}\right\} - \mathbb{E}_{\mathbf{\Phi}}\left\{\frac{\partial^2 \ln p_o(\mathbf{\Phi})}{\partial \mathbf{\Phi}^2}\right\} \\
&= \mathbb{E}_{\mathbf{\Phi}}\left\{-\mathbb{E}_{\mathbf{x}|\mathbf{\Phi}}\left\{\frac{\partial^2 \ln p(\mathbf{x}|\mathbf{\Phi})}{\partial \mathbf{\Phi}^2}\right\}\right\} - \mathbb{E}_{\mathbf{\Phi}}\left\{\frac{\partial^2 \ln p_o(\mathbf{\Phi})}{\partial \mathbf{\Phi}^2}\right\} \\
&= \mathbb{E}_{\mathbf{\Phi}}\{\mathbf{F}_l\} + \mathbf{F}_o.
\end{aligned} \tag{22}$$

Using the noise covariance, $\mathbf{F}_l = \mathbf{g}^T \mathbf{R}_n^{-1} \mathbf{g}$, with $\mathbf{g} = \frac{\partial \mathbf{f}(\mathbf{\Phi})}{\partial \mathbf{\Phi}}$ where

$$\frac{\partial r_q}{\partial \mathbf{\Phi}} = \left[\frac{x - x_q}{((x - x_q)^2 + (y - y_q)^2)^{1/2}}, \frac{y - y_q}{((x - x_q)^2 + (y - y_q)^2)^{1/2}}\right], \tag{23}$$

$$\frac{\partial \theta_q}{\partial \mathbf{\Phi}} = \left[\left(1 + \left(\frac{y - y_q}{x - x_q}\right)^2\right)^{-1} \frac{y_q - y}{x - x_q}, \left(1 + \left(\frac{y - y_q}{x - x_q}\right)^2\right)^{-1} \frac{1}{x - x_q}\right]. \tag{24}$$

Using the prior $\mathbf{\Phi} \sim N(\mathbf{\Phi}_o, \mathbf{R_o})$ yields $\mathbf{F}_o = \mathbf{R}_o^{-1}$. ■

Theorem 3.2 (Non-coherent processing BCRLB)**.** *Given the deterministic but unknown nuisance parameters $\boldsymbol{\alpha}$, the BCRLB of $\mathbf{\Phi}$ in case of non-coherent processing is conditioned on $\boldsymbol{\alpha}$ as*

$$\mathbf{F}_{\mathbf{\Phi}}^{-1} = \left(\mathbb{E}_{\mathbf{\Phi}}\left\{\mathbf{F}_{\mathbf{\Phi},\mathbf{\Phi}}\right\} + \mathbf{F}_o - \mathbb{E}_{\mathbf{\Phi}}\left\{\mathbf{F}_{\mathbf{\Phi},\boldsymbol{\alpha}}\right\} \mathbf{F}_{\boldsymbol{\alpha},\boldsymbol{\alpha}}^{-1} \mathbb{E}_{\mathbf{\Phi}}\left\{\mathbf{F}_{\boldsymbol{\alpha},\mathbf{\Phi}}\right\}\right)^{-1}. \tag{25}$$

Proof: The BCRLB conditioned on $\boldsymbol{\alpha}$ is

$$\mathbf{C}_{\mathbf{\Phi}|\boldsymbol{\alpha}} = \mathbb{E}_{\mathbf{x}_{nc},\mathbf{\Phi}|\boldsymbol{\alpha}}\{(\mathbf{\Phi} - \hat{\mathbf{\Phi}})(\mathbf{\Phi} - \hat{\mathbf{\Phi}})^T\} \succeq \mathbf{F}_{\mathbf{\Phi}}^{-1}. \tag{26}$$

The nuisance parameters make it difficult to directly arrive at the BCRLB of $\mathbf{\Phi}$. Therefore, we derive it from the BCRLB of $\mathbf{\Phi}_1$, which is a hybrid lower bound because of presence of both random and deterministic parameters. The BCRLB of $\mathbf{\Phi}_1$ is

$$\mathbf{C}_{\mathbf{\Phi}_1} = \mathbb{E}_{\mathbf{x}_{nc},\mathbf{\Phi}_1|\boldsymbol{\alpha}}\{(\mathbf{\Phi}_1 - \hat{\mathbf{\Phi}}_1)(\mathbf{\Phi}_1 - \hat{\mathbf{\Phi}}_1)^T\} \succeq \mathbf{F}^{-1}, \tag{27}$$

where $\mathbf{F} \triangleq \mathbb{E}_{\mathbf{\Phi}}\{\mathbf{F}_l\} + \mathbf{F}_p$ with

$$\mathbf{F}_l = -\mathbb{E}_{\mathbf{x}_{nc}|\mathbf{\Phi};\boldsymbol{\alpha}} \left\{ \frac{\partial^2 \ln p(\mathbf{x}_{nc}|\mathbf{\Phi};\boldsymbol{\alpha})}{\partial \mathbf{\Phi}_1^2} \right\}, \tag{28}$$

$$\mathbf{F}_p = -\mathbb{E}_{\mathbf{\Phi}_1} \left\{ \frac{\partial^2 \ln p_o(\mathbf{\Phi}_1)}{\partial \mathbf{\Phi}_1^2} \right\} = \begin{bmatrix} \mathbf{F}_o & \mathbf{0} \\ \mathbf{0} & \mathbf{0} \end{bmatrix}. \tag{29}$$

In block matrix form,

$$\mathbf{F}_l = \begin{bmatrix} \mathbf{F}_{\mathbf{\Phi},\mathbf{\Phi}} & \mathbf{F}_{\mathbf{\Phi},\boldsymbol{\alpha}} \\ \mathbf{F}_{\boldsymbol{\alpha},\mathbf{\Phi}} & \mathbf{F}_{\boldsymbol{\alpha},\boldsymbol{\alpha}} \end{bmatrix}, \tag{30}$$

so that

$$\mathbf{F} = \begin{bmatrix} \mathbb{E}_{\mathbf{\Phi}}\{\mathbf{F}_{\mathbf{\Phi},\mathbf{\Phi}}\} + \mathbf{F}_o & \mathbb{E}_{\mathbf{\Phi}}\{\mathbf{F}_{\mathbf{\Phi},\boldsymbol{\alpha}}\} \\ \mathbb{E}_{\mathbf{\Phi}}\{\mathbf{F}_{\boldsymbol{\alpha},\mathbf{\Phi}}\} & \mathbf{F}_{\boldsymbol{\alpha},\boldsymbol{\alpha}} \end{bmatrix}. \tag{31}$$

Taking the Shur complement of (31) completes the proof. ■

In order to evaluate (25), we need to explicitly derive (28). From (16), we have $\mathbf{u}_x \triangleq \frac{\partial \mathbf{h}(\mathbf{\Phi})}{\partial x} = \mathbf{h}(\mathbf{\Phi}) \circ \mathbf{G}_x(\mathbf{\Phi})$, with $\mathbf{G}_x(\mathbf{\Phi}) = [G_{1,1,1,1}, \cdots, G_{q,m,n,n_s}, \cdots, G_{Q,M,N,N_s}]$ such that

$$G_{q,m,n,n_s} = j2\pi \left(\frac{f_c^q}{c} + \frac{B_r t_{n_s}}{c} \right) \frac{\partial g_{q,m,n}}{\partial x}, \tag{32}$$

$$\frac{\partial g_{q,m,n}}{\partial x} = \frac{x - x_{q,n}}{((x_{q,n} - x)^2 + (y_{q,n} - y)^2)^{1/2}} + \frac{x - x_{q,m}}{((x_{q,m} - x)^2 + (y_{q,m} - y)^2)^{1/2}}. \tag{33}$$

$\mathbf{u}_y \triangleq \frac{\partial \mathbf{h}(\mathbf{\Phi})}{\partial y} = \mathbf{h}(\mathbf{\Phi}) \circ \mathbf{G}_y(\mathbf{\Phi})$ is defined similarly. Let $\mathbf{A} = diag\{\boldsymbol{\alpha} \otimes \mathbf{1}_{MNN_s}\}$ and $\mathbf{R}_A = E[\mathbf{A}\mathbf{R}_{nc}^{-1}\mathbf{A}]$. Assuming that the noise components over different radar sensors are i.i.d., the inverse of the noise covariance matrix is $\mathbf{R}_{nc}^{-1} = diag\{\mathbf{R}_{\mathbf{1},\mathbf{1}}^{-1}, \cdots, \mathbf{R}_{Q,Q}^{-1}\}$, where $\mathbf{R}_{q,q}^{-1}$ is the inverse of the noise covariance matrix of the q-th radar. We define $h_q(\mathbf{\Phi}) \triangleq \mathcal{S}_q(\mathbf{\Phi})$, meaning that $h_q(\mathbf{\Phi})$ consists of the rows as indexed in the set of $\mathcal{S}_q$ of $\mathbf{h}(\mathbf{\Phi})$, with $\mathcal{S}_q = \{(q-1)MNN_s + 1, \cdots, qMNN_s\}$. In other words, $\mathbf{h}_q(\mathbf{\Phi}) = [h_{q,1,1}(t_1), \cdots, h_{q,M,N}(t_{N_s})]^T$. Similarly, define $\mathbf{u}_x^q = \mathbf{u}_x(\mathcal{S}_q, 1)$ and $\mathbf{u}_y^q = \mathbf{u}_y(\mathcal{S}_q, 1)$. Then, the elements of likelihood Fisher information matrix $\mathbf{F}_l$ are $\mathbf{F}_l(x,x) = 2\mathbf{u}_x^H\mathbf{R}_A\mathbf{u}_x$, $\mathbf{F}_l(x,y) = 2\Re\{\mathbf{u}_x^H\mathbf{R}_A\mathbf{u}_y\}$, $\mathbf{F}_l(y,y) = 2\mathbf{u}_y^H\mathbf{R}_A\mathbf{u}_y$, $\mathbf{F}_l(x,\alpha_r^q) = 2\Re\{(\alpha_q\mathbf{u}_x^q)^H\mathbf{R}_{q,q}^{-1}\mathbf{h}_q(\mathbf{\Phi})\}$, $\mathbf{F}_l(y,\alpha_r^q) = 2\Re\{(\alpha_q\mathbf{u}_y^q)^H\mathbf{R}_{q,q}^{-1}\mathbf{h}(\mathbf{\Phi})\}$, $\mathbf{F}_l(x,\alpha_i^q) = 2\Im\{\mathbf{h}(\mathbf{\Phi})^H\mathbf{R}_{q,q}^{-1}(\alpha_q\mathbf{u}_x)\}$, $\mathbf{F}_l(y,\alpha_i^q) = 2\Im\{\mathbf{h}(\mathbf{\Phi})^H\mathbf{R}_{q,q}^{-1}(\alpha_q\mathbf{u}_y^q)\}$, $\mathbf{F}_l(\alpha_r^q,\alpha_r^q) = 2\mathbf{h}_q(\mathbf{\Phi})^H\mathbf{R}_{q,q}^{-1}\mathbf{h}_q(\mathbf{\Phi})$, $\mathbf{F}_l(\alpha_i^q,\alpha_i^q) = 2\mathbf{h}_q(\mathbf{\Phi})^H\mathbf{R}_{q,q}^{-1}\mathbf{h}_q(\mathbf{\Phi})$, and $\mathbf{F}_l(\alpha_r^q,\alpha_i^q) = \mathbf{F}_l(\alpha_r^{q_1},\alpha_r^{q_2}) = \mathbf{F}_l(\alpha_i^{q_1},\alpha_i^{q_2}) = \mathbf{F}_l(\alpha_r^{q_1},\alpha_i^{q_2}) = 0$.

Theorem 3.3 (Coherent processing BCRLB)**.** *Given the deterministic but unknown nuisance parameter α, the BCRLB of $\mathbf{\Phi}$ in case of coherent processing is conditioned on α as*

$$\mathbf{F}_{\mathbf{\Phi}}^{-1} = (\mathbb{E}_{\mathbf{\Phi}}\{\mathbf{F}_{\mathbf{\Phi},\mathbf{\Phi}}\} + \mathbf{F}_o - \mathbb{E}_{\mathbf{\Phi}}\{\mathbf{F}_{\mathbf{\Phi},\alpha}\}\mathbf{F}_{\alpha,\alpha}^{-1}\mathbb{E}_{\mathbf{\Phi}}\{\mathbf{F}_{\alpha,\mathbf{\Phi}}\})^{-1}. \tag{34}$$

Proof: The proof follows by substituting $\alpha_q = \alpha, q = 1, \cdots, Q$ in the BCRLB of non-coherent processing. ■

4. NUMERICAL EXPERIMENTS

We evaluated different performance bounds on the accuracy of position through numerical experiments. In particular, we compute the average of the bounds on positions, i.e.

$$\bar{\mathbf{F}}_{\mathbf{\Phi}} = \frac{\mathbf{F}_{\mathbf{\Phi}}^{-1}(x,x) + \mathbf{F}_{\mathbf{\Phi}}^{-1}(y,y)}{2}. \tag{35}$$

In all experiments, each MIMO radar has two transmitters and four receivers. The receive and transmit antennas are spaced at half-wavelength and two wavelengths, respectively. The center frequency is 77 GHz with signal bandwidth 150 MHz, chirp duration 5 μs and sampling frequency 10 MHz. We consider $Q = 3$ radars located at coordinates $[0,0]$ m, $[1,0]$ m, and $[2,0]$ m within the *ego-car* coordinate system. The input SNR is -30 dB. Based on the CRLBs of frequency and DOA, this SNR leads to range estimation accuracy of 0.06 m, and DOA estimation accuracy of 0.02° (at 45° DOA).

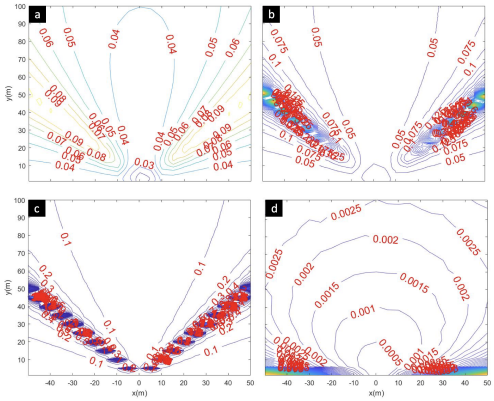

Fig. 2. Average bound on the position, i.e., $\bar{\mathbf{F}}_{\mathbf{\Phi}}$. (a) Point-cloud fusion BCRLB with $Q = 3$ radars, (b) Point-cloud fusion CRLB, $Q = 3$, (c) Point-cloud fusion CRLB, $Q = 1$, (d) Non-coherent processing BCRLB, $Q = 3$. The radars are located at $[0,0]$ m, $[1,0]$ m, and $[2,0]$ m. The $Q = 1$ case corresponds to the first radar.

Using only one radar sensor, the point-cloud fusion provides a location accuracy of about 0.1 m. The prior information on the target follows a Gaussian distribution centered at the true position and 0.1 m standard deviation. The target area of interest ranges $[-50, 50]$ m and $[0, 100]$ m in x- and y-dimensions. We numerically computed BCRLB conditions on the prior over 20 Monte-Carlo trials. Figure 2a and 2b show contours of the BCRLB and CRLB for point-cloud fusion using three radars while Fig. 2c plots CRLB of one radar with respect to the distance from radar sensors. We note that, when conventional processing is used without considering prior information, using three sensors significantly improves the performance of positioning accuracy over a single radar. Exploiting prior information provides additional improvement. Figure 2d illustrates BCRLB for, *ceteris paribus*, non-coherent processing with $Q = 3$ sensors; this mode significantly improves the accuracy of multiple displaced sensors. We further observed that the coherent processing (not shown for lack of space) outperforms the non-coherent mode by a very small margin.

5. SUMMARY

We studied three different displaced automotive sensor modes and their statistical performance bounds under unsynchronized clocks in a Bayesian framework. We noticed that the point-cloud fusion has improved performance over a single radar and conventional multiple displaced sensor imaging techniques. The non-coherent processing significantly outperforms point-cloud fusion in accuracy by an order of magnitude and is promising for future automotive systems.

6. REFERENCES

[1] F. Engels, P. Heidenreich, A. M. Zoubir, F. K. Jondral, and M. Wintermantel, "Advances in automotive radar: A framework on computationally efficient high-resolution frequency estimation," *IEEE Signal Processing Magazine*, vol. 34, no. 2, pp. 36–46, 2017.

[2] S. M. Patole, M. Torlak, D. Wang, and M. Ali, "Automotive radars: A review of signal processing techniques," *IEEE Signal Processing Magazine*, vol. 34, no. 2, pp. 22–35, 2017.

[3] Z. Slavik and K. V. Mishra, "Phenomenological modeling of millimeter-wave automotive radar," in *2019 URSI Asia-Pacific Radio Science Conference*, 2019, pp. 1–4.

[4] M. A. Richards, *Fundamentals of radar signal processing*. McGraw-Hill, 2005.

[5] K. V. Mishra, M. R. Bhavani Shankar, V. Koivunen, B. Ottersten, and S. A. Vorobyov, "Toward millimeter wave joint radar communications: A signal processing perspective," *IEEE Signal Processing Magazine*, vol. 36, pp. 100–114, 2019.

[6] A. Ayyar and K. V. Mishra, "Robust communications-centric coexistence for turbo-coded OFDM with non-traditional radar interference models," in *IEEE Radar Conference*, 2019, in press.

[7] H. H. Meinel, "Evolving automotive radar From the very beginnings into the future," in *IEEE European Conference on Antennas and Propagation*, 2014, pp. 3107–3114.

[8] Z. Slavik and K. V. Mishra, "Cognitive interference mitigation in automotive radars," in *IEEE Radar Conference*, 2019, in press.

[9] G. Duggal, S. Vishwakarma, K. V. Mishra, and S. S. Ram, "Doppler-resilient 802.11ad-based ultra-short range automotive radar," *arXiv preprint arXiv:1902.01306*, 2019.

[10] M. Steiner, T. Grebner, and C. Waldschmidt, "Chirp-sequence-based imaging using a network of distributed single-channel radar sensors," in *IEEE MTT-S International Conference on Microwaves for Intelligent Mobility*, 2019, pp. 1–4.

[11] A. Myakinkov, S. Sidorov, S. Shishanov, and S. Shabalin, "The distributed radar system for monitoring the surrounding situation for the intelligent vehicle," in *International Radar Symposium*, 2018, pp. 1–8.

[12] R. Mudumbai, D. R. B. Iii, U. Madhow, and H. V. Poor, "Distributed transmit beamforming: Challenges and recent progress," *IEEE Communications Magazine*, vol. 47, no. 2, pp. 102–110, 2009.

[13] Y.-S. Tu and G. J. Pottie, "Coherent cooperative transmission from multiple adjacent antennas to a distant stationary antenna through AWGN channels," in *IEEE Vehicular Technology Conference - Spring*, 2002, pp. 130–134.

[14] R. Chopra, C. R. Murthy, and R. Annavajjala, "Multistream distributed cophasing," *IEEE Transactions on Signal Processing*, vol. 65, no. 4, pp. 1042–1057, 2016.

[15] T. Tirer and A. J. Weiss, "High resolution direct position determination of radio frequency sources," *IEEE Signal Processing Letters*, vol. 23, no. 2, pp. 192–196, 2016.

[16] R. Karlsson and F. Gustafsson, "The future of automotive localization algorithms: Available, reliable, and scalable localization: Anywhere and anytime," *IEEE signal processing magazine*, vol. 34, no. 2, pp. 60–69, 2017.

[17] L. Cong and W. Zhuang, "Hybrid TDOA/AOA mobile user location for wideband CDMA cellular systems," *IEEE Transactions on Wireless Communications*, vol. 1, no. 3, pp. 439–447, 2002.

[18] K. Ho and Y. Chan, "Solution and performance analysis of geolocation by TDOA," *IEEE Transactions on Aerospace and Electronic Systems*, vol. 29, no. 4, pp. 1311–1322, 1993.

[19] Y. Chan and K. Ho, "A simple and efficient estimator for hyperbolic location," *IEEE Transactions on Signal Processing*, vol. 42, no. 38, pp. 1905–1915, 1994.

[20] A. J. Weiss and A. Amar, "Direct position determination of multiple radio signals," *EURASIP Journal on Advances in Signal Processing*, vol. 2005, no. 1, p. 653549, 2005.

[21] S. Roehr, M. Vossiek, and P. Gulden, "Method for high precision radar distance measurement and synchronization of wireless units," in *IEEE/MTT-S International Microwave Symposium*, 2007, pp. 1315–1318.

[22] G. Wang, C. Gao, S. G. Razul, and C. M. S. See, "A new direct position determination algorithm using multiple arrays," in *IEEE International Conference on Digital Signal Processing*, 2018, pp. 1–5.

[23] G. Wang, S. G. Razul, and C. M. See, "DOA estimation using multiple antenna arrays," in *IEEE Sensor Signal Processing for Defence Conference*, 2017, pp. 1–5.

[24] C. R. Berger and J. M. Moura, "Noncoherent compressive sensing with application to distributed radar," in *IEEE Annual Conference on Information Sciences and Systems*, 2011, pp. 1–6.

[25] M. Cho, K. V. Mishra, and W. Xu, "Computable performance guarantees for compressed sensing matrices," *EURASIP Journal on Advances in Signal Processing*, vol. 2018, no. 1, p. 16, 2018.

[26] D. Liu, U. S. Kamilov, and P. T. Boufounos, "Sparsity-driven distributed array imaging," in *IEEE International Workshop on Computational Advances in Multi-Sensor Adaptive Processing*, 2015, pp. 441–444.

[27] M. A. Lodhi, H. Mansour, and P. T. Boufounos, "Coherent radar imaging using unsynchronized distributed antennas," in *IEEE International Conference on Acoustics, Speech and Signal Processing*, 2019, pp. 4320–4324.

[28] S. Sun, K. V. Mishra, and A. P. Petropulu, "Target estimation by exploiting low rank structure in widely separated MIMO radar," in *IEEE Radar Conference*, 2019, pp. 1–5.

[29] *IEEE Standard for a Precision Clock Synchronization Protocol for Networked Measurement and Control Systems*, 2008, IEEE Std 1588-2008 (Revision of IEEE Std 1588-2002).

[30] Y. Rockah and P. Schultheiss, "Array shape calibration using sources in unknown locations - Part I: Far-field sources," *IEEE Transactions on Acoustics, Speech, and Signal Processing*, vol. 35, no. 3, pp. 286–299, 1987.

[31] Y. Noam and H. Messer, "Notes on the tightness of the hybrid Cramér-Rao lower bound," *IEEE Transactions on Signal Processing*, vol. 57, no. 6, pp. 2074–2084, 2009.

[32] M. A. Kumar and K. V. Mishra, "Information geometric approach to Bayesian lower error bounds," in *IEEE International Symposium on Information Theory*, 2018, pp. 746–750.

[33] K. V. Mishra and Y. C. Eldar, "Performance of time delay estimation in a cognitive radar," in *IEEE International Conference on Acoustics, Speech and Signal Processing*, 2017, pp. 3141–3145.

[34] K. V. Mishra and Z. Slavik, "ReMCW: Reduced bandwidth FMCW radar for autonomous driving," in *IEEE Asilomar Conference on Signals, Systems, and Computers*, 2019, in press.

[35] M. I. Skolnik, *Radar handbook*, 3rd ed. McGraw-Hill, 2008.

[36] P. Tichavský, C. H. Muravchik, and A. Nehorai, "Posterior Cramér-Rao bounds for discrete-time nonlinear filtering," *IEEE Transactions on Signal Processing*, vol. 46, no. 5, pp. 1386–1396, 1998.